Raman spectroscopy of gallium ion irradiated graphene

Raman Spectroscopy of Gallium Ion Irradiated Graphene

Anthea Agius Anastasi*, Andrea Valsesia, Pascal Colpo, Matthew K. Borg and Glenn Cassar

Abstract

The successful integration of graphene in future technologies, such as filtration and nanoelectronics, depends on the ability to introduce controlled nanostructured defects in graphene. In this work, Raman spectroscopy is used to investigate the induction of disorder in graphene via gallium ion beam bombardment. Two configurations of CVD-grown graphene samples are used: (i) graphene supported on a Si/SiO_2 substrate, and (ii) graphene suspended on porous TEM grids. It is observed that the supported graphene experiences more damage in response to lower beam doses than suspended graphene. This phenomenon is attributed to the behaviour of the energetic ions impinging the sample. In suspended graphene, the ions pass through the graphene membrane once and disperse to the atmosphere, while in supported graphene, the ions embed themselves in the substrate causing swelling and backscattering events, hence increasing the induced disorder. In supported graphene, the ratio between the Gaussian D and G peaks attributed to amorphous carbon, and the Lorentzian D and G peaks attributed to graphene, (I_{DG}/I_{DL}) and (I_{GG}/I_{GL}), are suggested to be used to quantify the degree of amorphization. The results are relevant to the development of nanostructured graphene-based filtration or desalination membranes, as well as for graphene-based nanoelectronics.

1. Introduction

Understanding the nature of defects in graphene is key to the effective integration of graphene in several dedicated applications. Focused electron and ion beams have been used to introduce point defects, nanopores, or nanopatterned graphene structures. These nanostructures are in turn of great interest for use in next-generation desalination membranes whereby the nanoporous graphene can act as a filtration membrane [1, 2], and nanoelectronics which often require

* Corresponding author. E-mail: anthea.agius-anastasi@um.edu.mt

graphene to be nanopatterned in specific geometries [2]. In the quest to realise these applications, significant work has been done to develop and establish an effective technique for graphene characterisation. To this end, Raman spectroscopy has been successfully used to positively identify graphene [1] and determine the number of carbon atom layers in it [1, 3, 4]. Furthermore, Raman spectroscopy can be used to study the extent and type of defects present in graphene [3, 5-7]. While the effect of different energetic particle beam parameters on supported graphene has been studied by Raman spectroscopy [2, 5, 8-12], the effects of such energetic particle bombardment on suspended graphene, i.e. unsupported graphene in the form of membranes, is less so investigated [7, 13, 14]. Furthermore, the immediate area surrounding the location directly irradiated by the beam may also be of significant interest due to the resulting damage profile [10].

In this work, the effects of gallium ion bombardment on both supported and suspended graphene is investigated. CVD-grown graphene supported on a Si/SiO_2 substrate is patterned with a focused gallium ion beam, while the surrounding area and the concomitant damage profile are characterized by Raman spectroscopy. The Raman spectra taken at various distances from the directly irradiated area are used to indicate the extent of damage imparted on graphene. In the second part of this study, freely suspended CVD-grown graphene membranes are also exposed to gallium ion treatments at different ion beam parameters, with Raman spectroscopy used to characterize the extent of damage imparted on the suspended graphene.

2. Experimental Study

2.1 Supported Graphene

Single layer graphene (nominal thickness and grain size 0.345 nm and 1 mm, respectively [15]) grown via chemical vapour deposition (CVD) and transferred on to SiO_2 substrate (Graphene on SiO_2, supplied by Nano Carbon Sp. z o.o.) was patterned by a focused gallium ion beam at an accelerating voltage of 5 kV and ion beam current of 47 pA, using a FEI Nova600 Dual Beam. Five different beam doses, ranging from 1.8×10^{-13} up to 1×10^{-10} C/μm^2 (equivalent to 1.12×10^{6} to 6.24×10^{8} $Ga^+/\mu m^2$) as listed in Table 1, were used to pattern different areas in the graphene sample.

2.2 Suspended Graphene

CVD-grown monolayer graphene membranes (nominal thickness and grain size 0.345 nm and 10 µm, respectively [16]) suspended over Quantifoil TEM mesh grids with 2 µm diameter holes (Suspended Monolayer Graphene on TEM grids - Quantifoil R2/4, supplied by Agar Scientific Ltd., UK) were subjected to focused gallium ion beam bombardment using the same FEI Nova600 Dual Beam. The conditions of the ion beam for each treatment are listed in Table 1. To achieve different treatment doses, the pitch of the ion beam raster was changed. A total of four TEM grids were available, only three of which being exposed to the gallium ion treatment.

Table 1: Focused Gallium Ion Beam Treatments on Supported Graphene and Suspended Graphene.

Sample	Energy (kV)	Current (pA)	Incidence Angle (°)	Dose (C/µm^2)		Fluence (Ga^+/µm^2)
Supported Graphene	5.0	47	90	1.80×10^{-13}	(T0.18)	1.12×10^{6}
				5.00×10^{-13}	(T0.5)	3.12×10^{6}
				1.00×10^{-12}	(T1)	6.24×10^{6}
				5.00×10^{-11}	(T50)	3.12×10^{8}
				1.00×10^{-10}	(T100)	6.24×10^{8}
Suspended Graphene	5.0	1.6	90	5.28×10^{-7}		3.30×10^{12}
				5.28×10^{-5}		3.30×10^{14}
				2.11×10^{-4}		1.32×10^{15}
				4.86×10^{-4}		3.03×10^{15}
				5.28×10^{-3}		3.30×10^{16}
				1.22×10^{-2}		7.62×10^{16}
	30.0	1.5	90	3.27×10^{-7}		2.04×10^{12}
				3.27×10^{-3}		2.04×10^{16}
				1.31×10^{-2}		8.18×10^{16}
	30.0	1.5	28	3.27×10^{-3}		2.04×10^{16}
			53			
			68			
			83			

2.3 Characterization

Scanning electron microscopy (SEM) (Zeiss Merlin Gemini, Germany) and atomic force microscopy (AFM) (UHV SPM700, RHK Inc., USA) were used to study the topography of the graphene. Electron dispersive spectroscopy (EDS) (Apollo X Ametek, USA) was also used to assess the elemental composition of the samples.

Raman spectroscopy (Witec Alpha300) with an excitation wavelength of 633 nm (1.9587 eV), a 60x objective, and a 600 g/mm grating was used to characterise the graphene. Raman spectra were recorded from the untreated and treated areas to compare the quality of graphene before and after ion beam bombardment. For the supported graphene, the damaged graphene surrounding the treated areas was also analysed, with the distance away from the edge of the 1×10^{-10} C/μm^2 treated area, *R*, ranging from 0 to 66 μm (denoted as $T100_0$ to $T100_{60}$, respectively), in steps of 6.6 μm.

Both single spectra and 2D spectral maps were gathered for each treated area. For the single spectra, an integration time of 10 seconds was used for a total of 10 accumulations. For the 2D spectral maps (a sample of which is included in the Supporting Information), an integration time of 5 seconds was used with an acquisition step size varying from 0.1 to 0.5 μm. For each map, sets of ten consecutive spectra obtained from circular areas of freely suspended graphene, and hence those featuring minimal substrate-generated background noise, were selected and averaged.

To eliminate background noise due to fluorescence, a 2nd order polynomial for supported graphene, or a 3rd order polynomial for suspended graphene, was fitted using the modified polyfit method outlined in [17] after manually removing sporadic spikes associated with cosmic rays from the raw spectra. An additional weighting function was added to the fitting procedure to improve the polynomial fit and better represent the less-active regions, namely < 1000 cm^{-1}, between 1600 cm^{-1} and 2500 cm^{-1}, and > 2750 cm^{-1}. The above-outlined mathematical processing was performed using Matlab (The MathWorks Inc., MA). The program used is available in the Supporting Information.

The Peak Analyzer in OriginPro 9 software was used to fit the peaks in the Raman spectra. The majority of the fits have a χ^2 value smaller than 3×10^{-3} and an adjusted R^2 value larger than 0.9. For clarity, the peak position or frequency, intensity, full width at half maximum (FWHM), and integrated area will be denoted by *P*, *I*, *F*, and *A*, respectively, while subscripts indicate the peak i.e. *D*, *G* or *2D*.

3. Results

3.1 Untreated Supported Graphene

Several Raman measurements were taken at different areas of the untreated supported CVD graphene, with the spectra obtained mainly falling into two categories. Representative spectra of each category are shown in Figure 1.

Both types of spectra have sharp Lorentzian profiles for the G and 2D peaks, the latter indicating the presence of single layer graphene. The G peak is found at around 1595 cm^{-1}, and has a FWHM of ~14 cm^{-1}. The 2D peak is found at ~2652 cm^{-1} with a FWHM of ~35 cm^{-1}.

The sharpness of the 2D peak, as well as the high 2D to G peak intensity ratio (I_{2D}/I_G) of around 2.5 (Figure 1 (b)) is indicative of monolayer graphene [1, 3]. In some areas of the same CVD graphene sample, a relatively low I_{2D}/I_G of around 0.87 (Figure 1 (a)) suggests the presence of multiple layers. The latter notion is further supported by the work of Reina et al. [4], suggesting that in few-layer CVD graphene the stacking order typical of highly ordered pyrolytic graphite might not be preserved, hence stacked graphene layers might still have a sharp 2D peak with a single Lorentzian line shape rather than a superposition of multiple peaks [18, 19]. Thus, it has been subsequently determined that the I_{2D}/I_G ratio is indeed a better indication of the number of layers in CVD graphene rather than the profile of the 2D peak, suggesting that an I_{2D}/I_G of ~0.76 corresponds to ~3 layers [4].

The main difference between the two types of graphene found on the same sample lies in the disorder-activated D peak at around 1332 cm^{-1}. While the spectrum shown in Figure 1 (a) has a low I_D/I_G of 0.096, an appreciable I_D/I_G of 1.19 was detected in certain areas such as shown in Figure 1 (b). The D+D" peak is also detected at 2468 cm^{-1}. This indicates that the untreated graphene has few defects, most likely limited to domain boundaries and wrinkles often present in CVD graphene. Representative SEM images of the untreated supported CVD graphene are shown in the Supporting Information, clearly highlighting the presence of grain boundaries and areas of bi- or multilayer graphene, or other contaminants. EDS analysis on different areas resulted in inconclusive results since the EDS signal detected mainly corresponds to the substrate much more than the top-surface layers. Furthermore, sensitivity to carbon at the surface is not adequate to indicate the presence and quality of graphene.

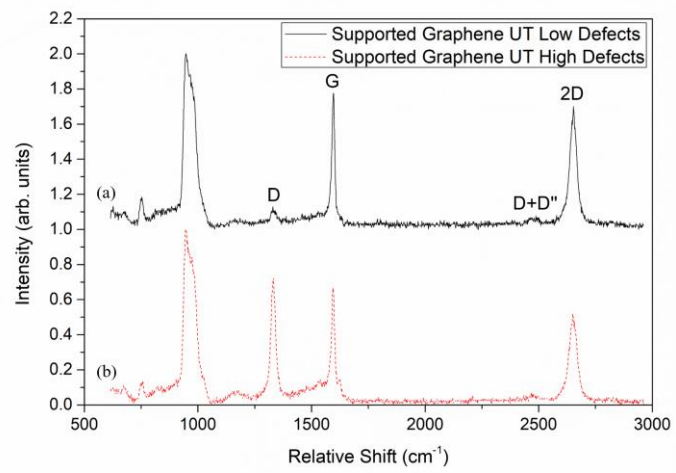

Figure 1: Untreated (UT) supported graphene. (a) The top solid black line is representative of areas with a small D peak, while (b) the bottom dashed red line is representative of areas with a larger D peak.

3.2 Untreated Suspended Graphene

A representative Raman spectrum of the untreated suspended CVD graphene is shown in Figure 2. A sharp single Lorentzian 2D peak at around 2635 cm^{-1} with a FWHM of ~36 cm^{-1} and a large I_{2D}/I_G of ~1.8 is characteristic of single layer graphene. Two additional Gaussian peaks were fitted for the D and G bands. Some areas of the untreated graphene membrane had a small Lorentzian D peak at ~1323 cm^{-1} and an I_D/I_G intensity ratio not exceeding 0.9. Similar to the supported graphene, the detection of this defect-activated Raman band as well as the Gaussian peaks are attributed to the presence of wrinkles, grain boundaries, areas of bi-layer graphene and possibly contaminants that have been introduced to the graphene membranes during transfer, all of which common for transferred CVD-grown graphene membranes. This is further supported by the SEM image of a representative graphene membrane, shown in Figure 3 (a), where brighter areas indicate the presence of folded/multilayer graphene, or grain boundaries. Non-contact AFM imaging, Figure 3 (b) also confirm the presence of wrinkles in the graphene membrane.

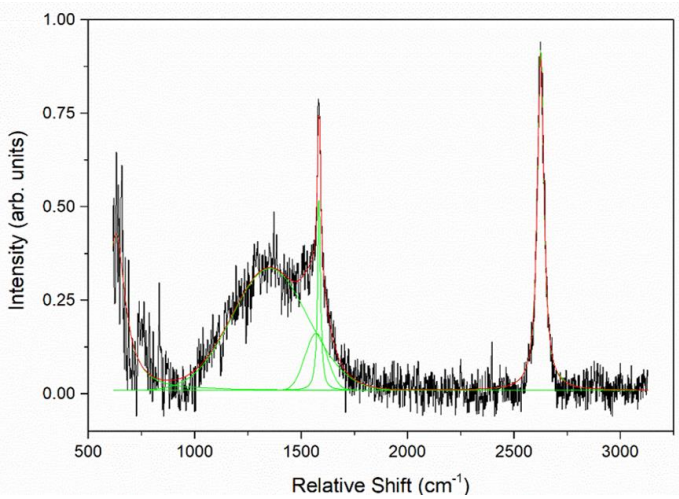

Figure 2: Representative Raman spectrum of untreated suspended graphene.

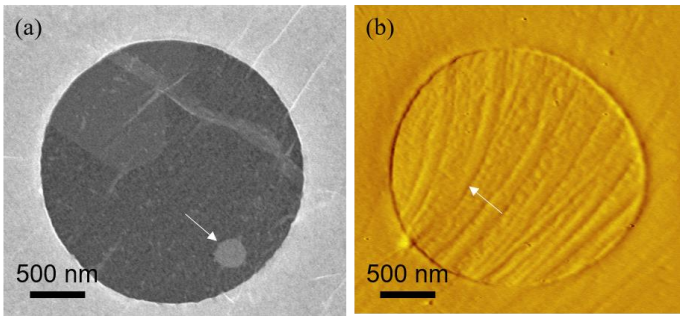

Figure 3: (a) SEM and (b) AFM images of the untreated suspended graphene membranes showing several wrinkles, grain boundaries and areas of bi-layer graphene.

3.3 Treated Supported Graphene

Figure 4 (a) shows an SEM image of the treated supported CVD graphene. A two-dimensional Raman spectral map was obtained to cover the entire treated area. Figure 4 (b-e) show the same spectral map with the intensity colour of each pixel corresponding to the intensity of part of the corresponding spectrum. For example, while Figure 4 (c) shows the intensity of the D peak (between 1290.8 and 1368.8 cm^{-1}), Figure 4 (e) shows the intensity of the 2D peak (between 2583.3 and 2717.0 cm^{-1}). Generally, the brighter the area is on the D peak map, the darker it is on the 2D peak map, yet in some instances, some brightness can be attributed to fluorescence.

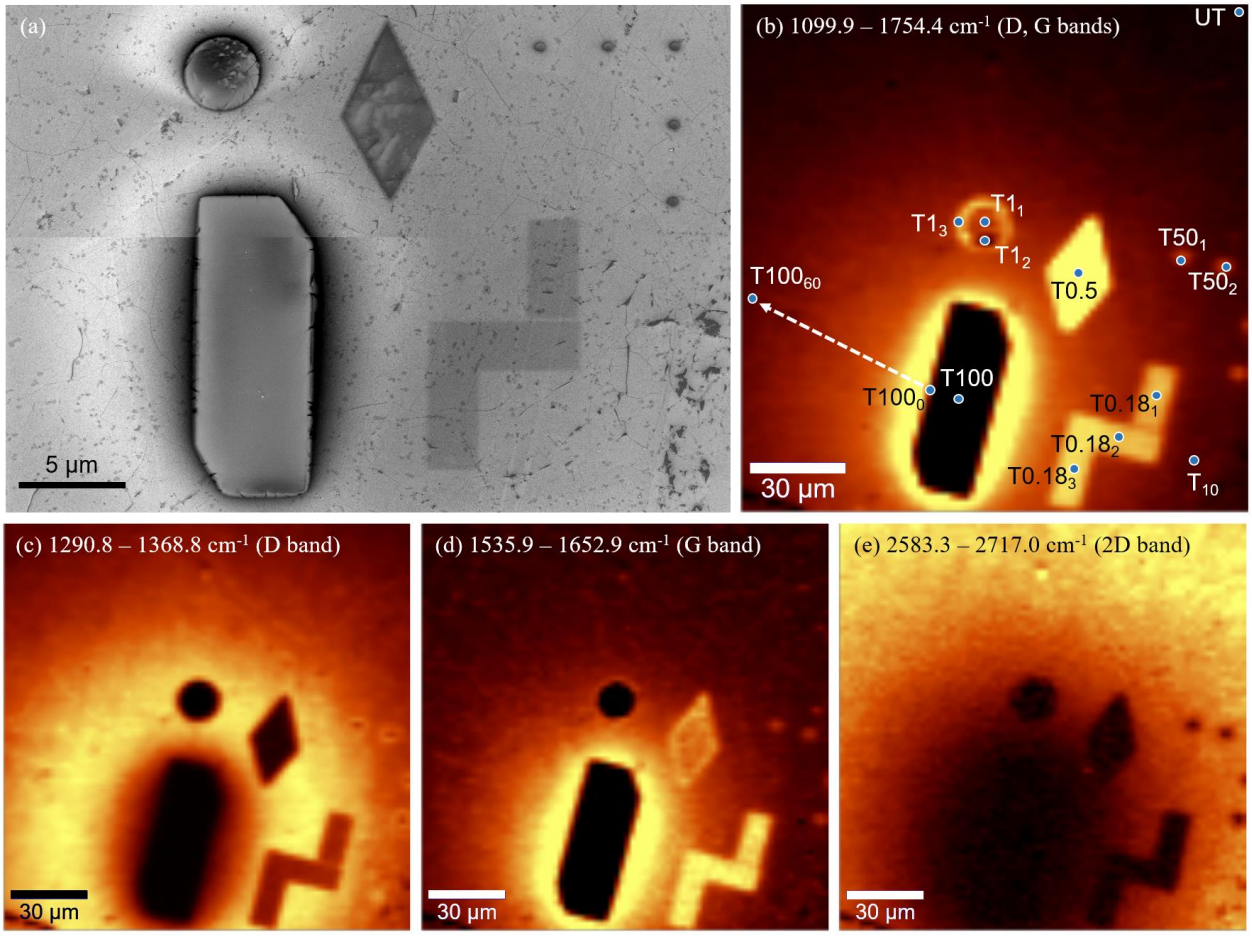

Figure 4: Treated supported CVD graphene patterned via a focused gallium ion beam. (a) SEM image. In (b), T0.18, T0.5 etc. represent the areas treated with a dose of 0.18 pC/µm^2 and 0.5 pC/µm^2 etc., respectively, while the subscripts refer to the repeated readings. For the case of T100 (area treated with 100 pC/µm^2), the subscripts represent the distance away from the edge of the 100 pC/µm^2 area in micrometres, *R*. (b-e) 2D Raman spectral maps of the sum of parts of the spectrum. The intensity colour of each map (b-e) represents the intensity of the spectrum at each pixel between the Raman shifts as indicated in the parenthesis on each image. For example, in (b), the intensity of the D and G bands, between 1099.9 and 1754.4 cm^{-1}, is mapped, with the brighter colours representing higher intensities.

The SEM image in Figure 4 (a) shows that the areas treated with 1×10^{-12} C/µm^2 (T1) and 5×10^{-13} C/µm^2 (T0.5) are damaged, with the former appearing more damaged. The texture, while not entirely flat and featureless like in the case of the two higher doses (T50 and T100), is still different than the rest of the untreated graphene, mainly characterised by uneven brightness. The Raman spectra indicate that while the 2D peak is absent from both areas, significantly broad (large FWHM) D and G peaks may appear in only some parts. In other areas, the broadened D

and G peaks merge to form one plateaued peak. Finally, a dose of 1.8×10^{-13} C/μm^2 (T0.18) retained the texture of the untreated graphene and the SEM only registered a change in the brightness in the treated area. However, the 2D peak is still barely present while the D and G peaks are significantly large yet less broad and more defined than at higher doses.

The Raman spectrum recorded from the directly irradiated area with an ion beam dose of 1×10^{-10} C/μm^2 (T100) is free from any peaks characteristic of graphene or other carbonaceous materials, signifying the complete removal of graphitic material during ion bombardment. The area surrounding the 1×10^{-10} C/μm^2 (T100) and 1×10^{-12} C/μm^2 (T1) treated areas also looks damaged in the SEM images by the presence of a dark ring followed by a bright ring around the target areas. Moreover, the 2D Raman maps reveal a larger radius of damage (up to around 70 μm from the target areas) caused by the treatment evident from a circular ring of low 2D peaks (Figure 4 (e)) and large D peaks (Figure 4 (c)). This surrounding area and the associated damage profile were investigated, and the recorded Raman spectra are presented.

At the edge of the bombarded area (R = 0 μm, $T100_0$ in Figure 4 (b)), the D+D" and 2D band disappear, while the Lorentzian D and G bands downshift by 16 cm^{-1} and 20 cm^{-1}, respectively as shown in Figure 5. As the Raman spectra were taken further away from the irradiated area, the untreated graphene spectrum was progressively restored. Thus, as shown in Figure 5 and Figure 6, the position of the Lorentzian D, G, and 2D peaks upshift slowly converging toward the original positions in untreated graphene, in agreement with [9]. The intensity of the 2D peak linearly increases while the FWHM of the 2D peak non-linearly decreases further away from the edge of the treated area. This combination causes the integrated area of the 2D peak to exhibit non-monotonic behaviour as shown in Figure 6.

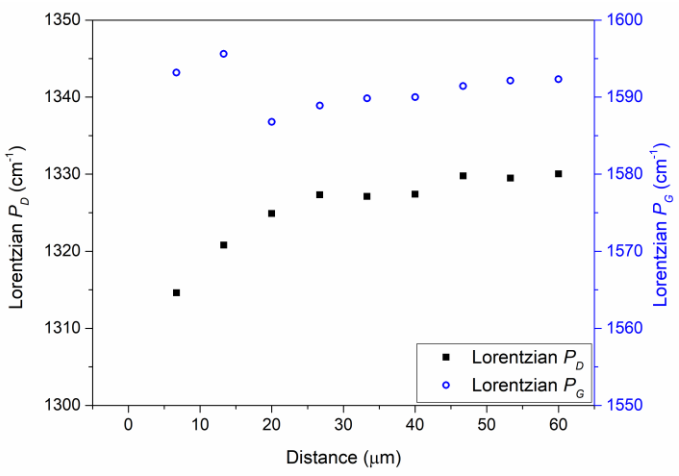

Figure 5: The evolution of the position of the Lorentzian D band (P_D) and Lorentzian G band (P_G) in the damaged supported graphene.

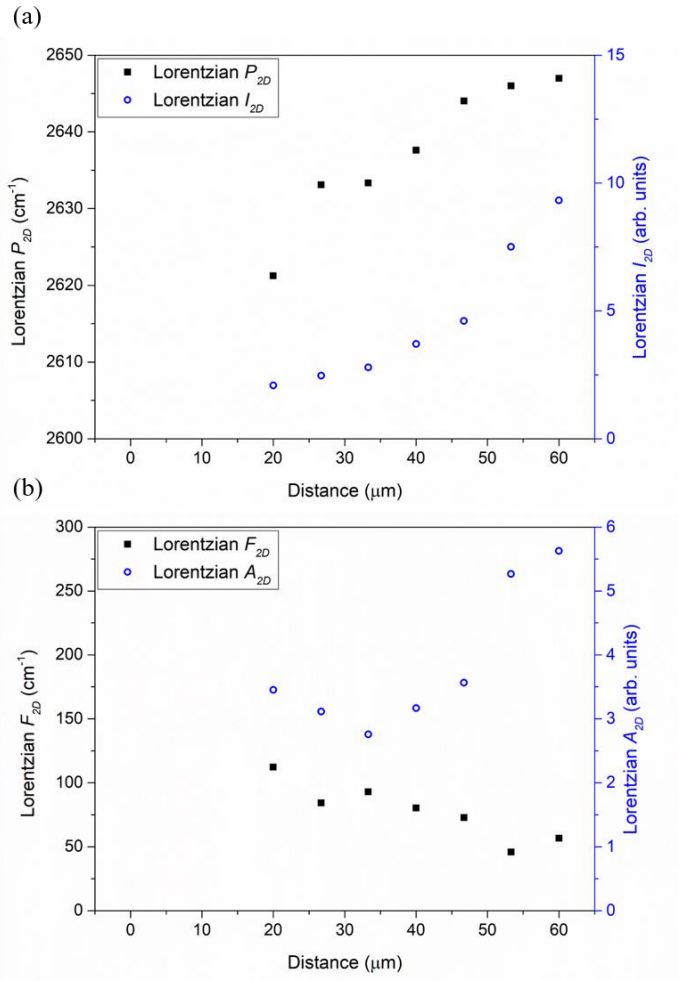

Figure 6: The evolution of the 2D band in the damaged supported graphene.

Particularly in Raman spectra taken from areas closer to the directly treated area, it was noted that the profiles of both the D and G peak are not entirely Gaussian nor Lorentzian. As such, the D and G peaks of such spectra of supported highly-damaged graphene were fit with two components each; a Lorentzian peak for crystalline graphene and a Gaussian peak to represent the partial amorphization of graphene. In fact, the Raman spectrum corresponds to amorphous carbon at the very edge of the treated area, with the Gaussian G peak appearing at 1571 cm^{-1} and the Gaussian D peak appearing at 1320 cm^{-1}. For R smaller than around 20 μm, both the Gaussian D peak and the Gaussian G peak increase in intensity and broaden indicating the large degree of amorphization (Figure 7). Both Gaussian peaks reduce in intensity and width with an increase in the distance from the edge of the treated area. This indicates that the amount of amorphous carbon present is reducing. The position of both the Gaussian G peak and of the Gaussian D peak is also observed to downshift further away from the directly treated area. This supports the assigning of these peaks to the amorphization of graphene, with an increase in the disorder of the sp^2 hybridized sites and an increase in the sp^3 hybridization resulting in a corresponding upshift of the Gaussian D and G peaks [20, 21]. Contrarily, the Lorentzian D peak and the intensity ratio between the Lorentzian D peak and the Lorentzian G peak (Lorentzian I_D/I_G) start to increase due to the larger presence of defected graphene rather than amorphous carbon (Figure 8).

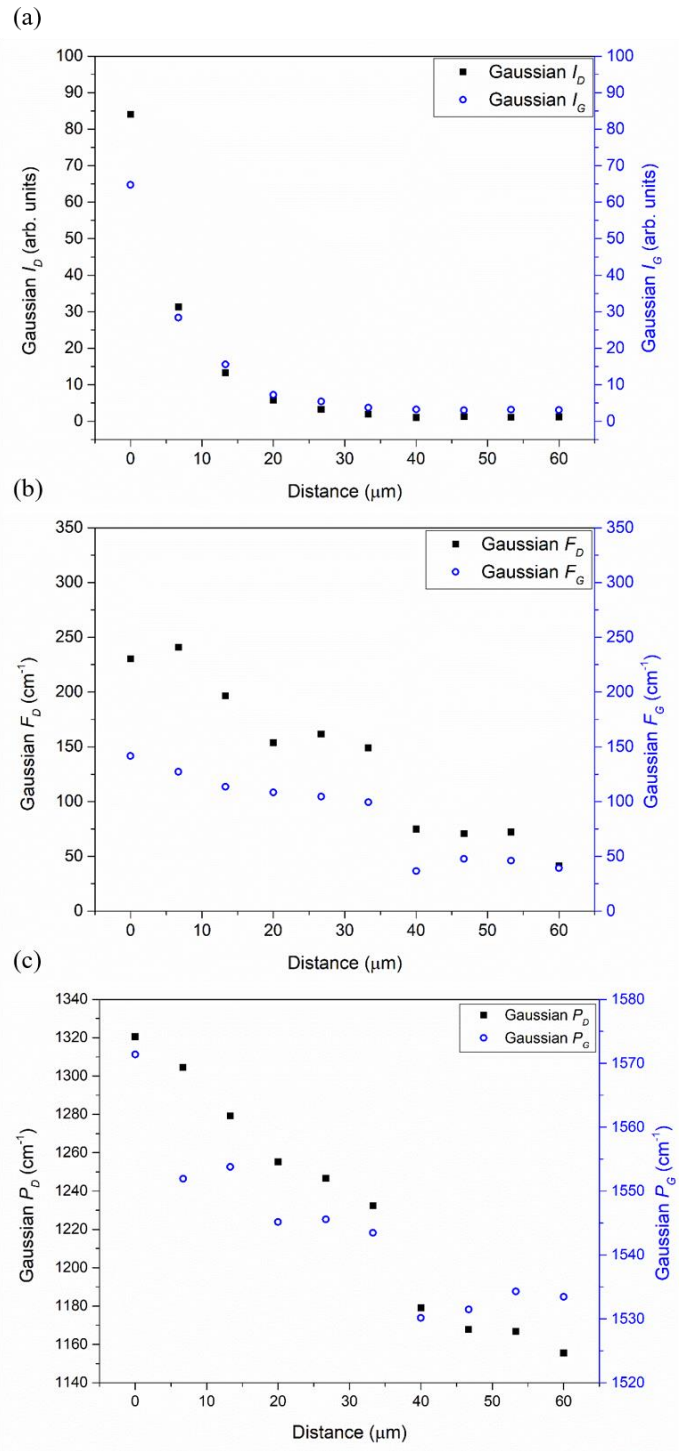

Figure 7: The evolution of the (a) intensity, (b) FWHM, and (c) position of the Gaussian D and Gaussian G bands in the damaged supported graphene.

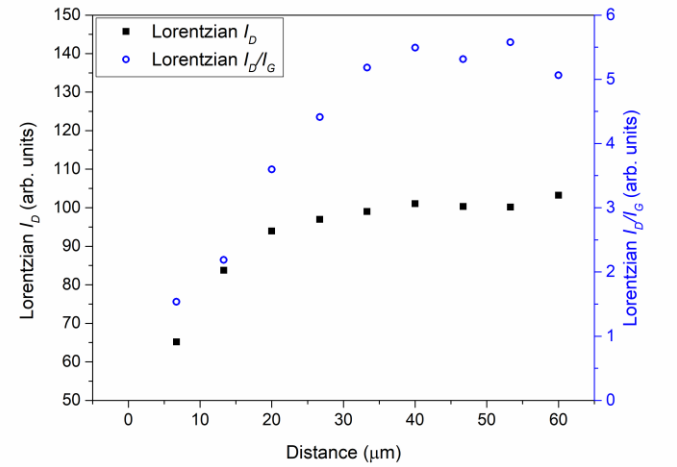

Figure 8: The evolution of the intensity of the Lorentzian D band (I_D) and the intensity ratio between the Lorentzian D band and Lorentzian G band (I_D/I_G) in the damaged supported graphene.

As shown in Figure 9, the intensity ratio between the Gaussian D peak and the Lorentzian D peak (I_{DG}/I_{DL}) is around 0.3 as close as 6.7 μm away from the edge of the treated area, and exponentially decays to around 0.01 at a distance of around 35 μm, where the ratio seems to stabilize over the next few micrometers. It is expected that this ratio continues to fall further away from the treated area to approach that for untreated CVD graphene. Likewise, the intensity ratio between the Gaussian D peak and the Gaussian G peak (I_{GG}/I_{GL}) is around 0.4 at around 13 μm, exponentially decays and finally stabilizes to around 0.16 at 45 μm. These two ratios are believed to be closely related to the degree of amorphization of graphene due to ion bombardment and the resulting high degree of disorder. Thus, it is suggested that in such cases of partial amorphization of graphene, the intensity ratios of the Gaussian D peak to the Lorentzian D peak (I_{DG}/I_{DL}) and the Gaussian G peak to the Lorentzian G peak (I_{GG}/I_{GL}) can be used to specify the degree of amorphization, with larger ratios indicating a higher degree of disorder.

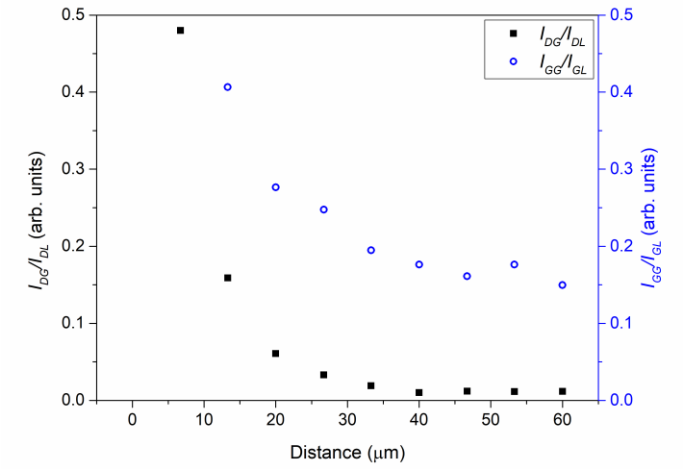

Figure 9: The evolution of the intensity ratio between the Gaussian and Lorentzian D band (I_{DG}/I_{DL}) and the intensity ratio between the Gaussian and Lorentzian G band (I_{GG}/I_{GL}) in the damaged supported graphene.

Figure 10 shows the Raman spectrum recorded at R = 40 μm. Raman spectra with similar peaks were recorded at R = 20 to 60 μm. Apart from the large Lorentzian I_D/I_G ratio, the presence of a low-intensity 2D peak and the Gaussian G peak previously attributed to the amorphous carbon, the Lorentzian G band is seen to split into two peaks with the emergence of the D' peak at around 1620 cm^{-1}. Although the Gaussian G peak (at around 1530 cm^{-1}) was previously attributed to the presence of amorphous carbon, the peak shape develops from a Gaussian one at higher defect concentrations to a Lorentzian peak shape.

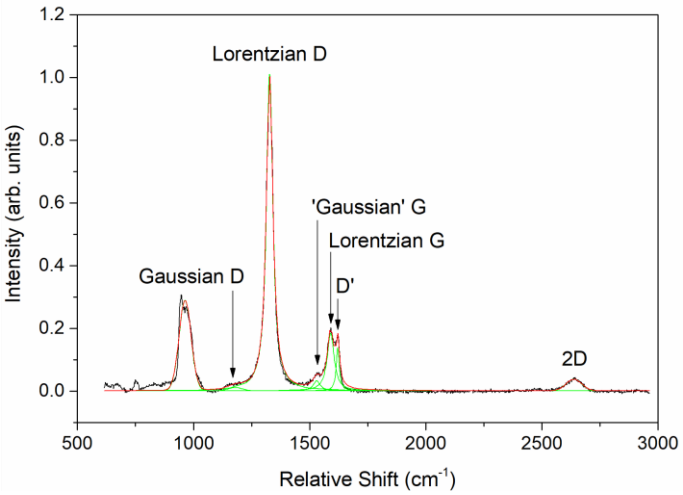

Figure 10: The Raman spectrum at R = 40 μm showing the D peak (1327.4 cm^{-1}), 'Gaussian G' peak (1530.1 cm^{-1}), Lorentzian G peak (1590.0 cm^{-1}), D' peak (1620.68 cm^{-1}) and 2D peak (2637.7 cm^{-1}).

Within the first 60 μm, the D peak is not fully restored, unlike the G peak whose intensity, position and FWHM significantly approach the pristine state after 42 μm.

3.4 Treated Suspended Graphene Membranes

Figures 11 to 13 show the peak parameters of interest for the Lorentzian and Gaussian D, G and 2D bands in treated suspended graphene. As expected, the intensity of the Lorentzian D band increases linearly with an increase in treatment dose (Figure 11 (b)). The Lorentzian D peak is also seen to downshift nonlinearly from around 1355 cm^{-1} to around 1325 cm^{-1} in an exponential decay (Figure 12 (a)). The frequencies at which the Lorentzian G band and 2D band occur do not shift significantly with the increase in treatment dose. However, both the Gaussian G band and Gaussian D band are seen to upshift with an increase in treatment dose, and downshift again at doses higher than 1.22×10^{-2} $C/\mu m^2$. The intensity of both the Lorentzian G and 2D bands linearly decrease with an increase in dose. However, changes in both parameters, especially the intensity of the 2D may not be statistically significant given the large variation in the untreated membranes. Since the intensity of the 2D peak decreases and the width of the same 2D peak exhibits no significant change, the integrated area of the 2D peak decreases with an increase in the treatment dose (Figure 13).

Figure 13 (b) shows the change in the Lorentzian I_D/I_G and F_D/F_G ratios of the suspended CVD graphene before and after gallium ion irradiation. The fact that the I_D increases while the I_G decreases enhances the linear increase of the I_D/I_G intensity ratio. The F_D/F_G follows an exponential decay mainly due to the changes of the same nature in the D peak.

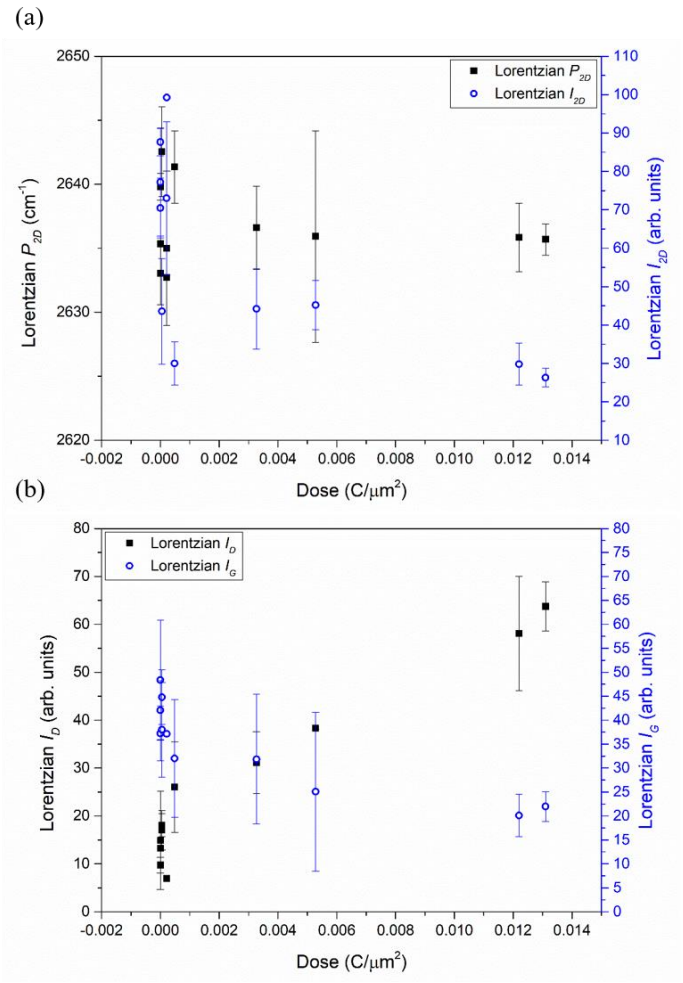

Figure 11: The evolution of (a) the position and intensity of the Lorentzian 2D peak, and (b) the intensities of the Lorentzian D and G peaks, in suspended graphene.

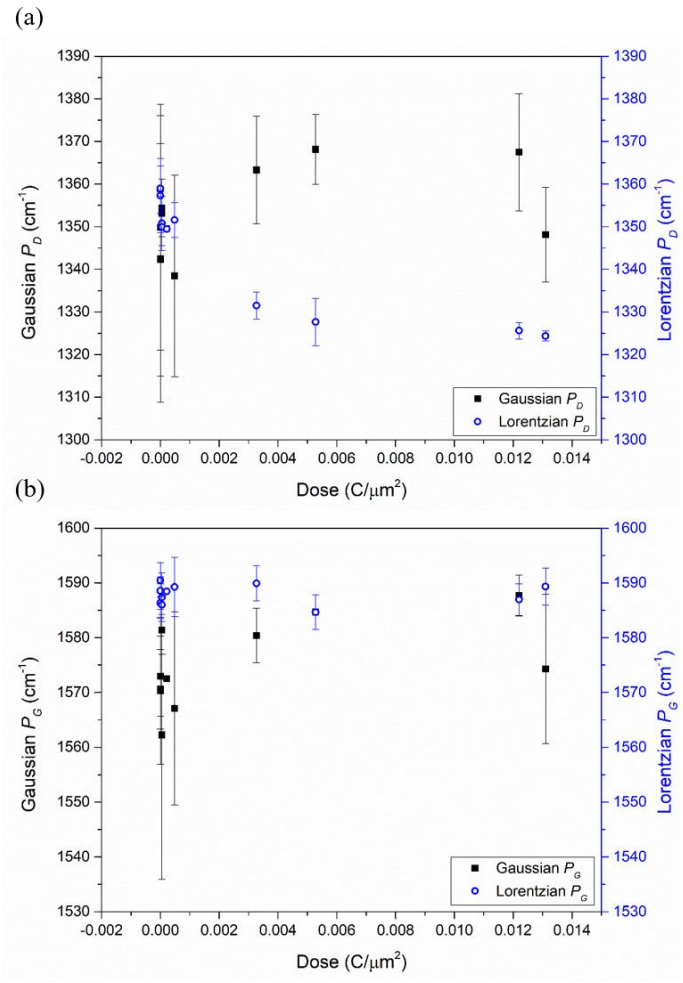

Figure 12: The evolution of the position of the Lorentzian and Gaussian (a) D peak, and (b) G peak, in suspended graphene.

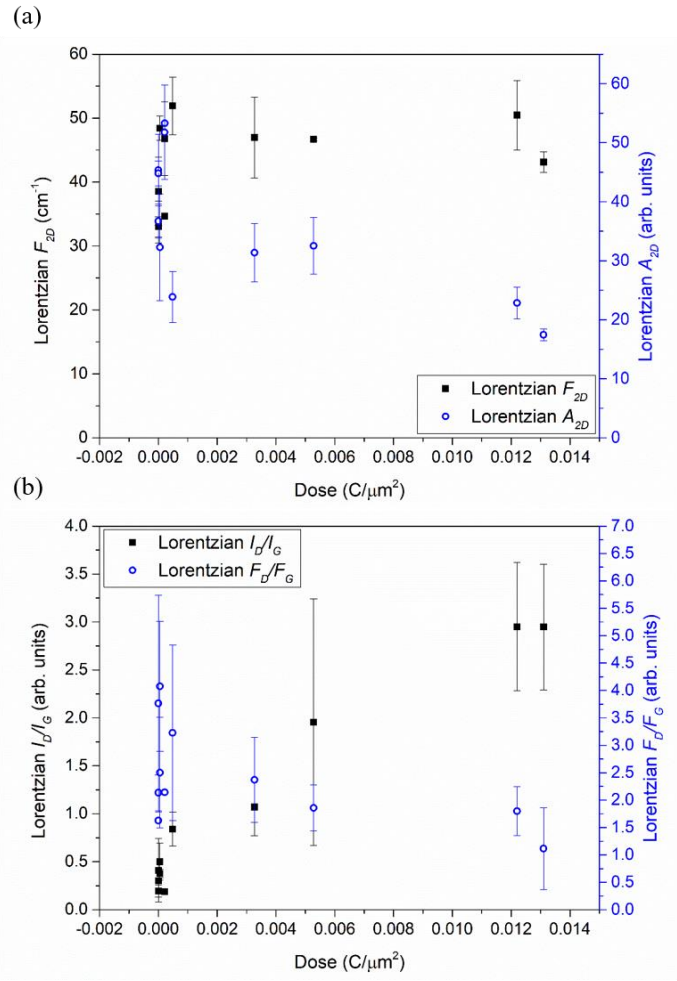

Figure 13: The evolution of (a) the FWHM and integrated area of the Lorentzian 2D peak, and (b) the intensity ratio I_D/I_G and FWHM ratio F_D/F_G, in suspended graphene.

The effect of the incidence angle on the Raman spectrum was also investigated. Only the 2D peak was not affected by the incidence angle. Similar to an increase in treatment dose, an increase in the incidence angle to the surface downshifted the Lorentzian D peak in an exponential decay from around 1355 cm^{-1} to around 1325 cm^{-1} (Figure 14). Furthermore, while the I_D increases linearly with a higher incidence angle (i.e. closer to normal incidence), the F_D decreases linearly from around 40 cm^{-1} to 20 cm^{-1}, causing the overall area to decrease. Again, similar to the treatment dose, an increase in the angle of incidence appears to some extent reduce the F_G and hence the A_G (Figure 15). The abovementioned changes cause the I_D/I_G ratio in Figure 16 to increase linearly with an increase in incidence angle.

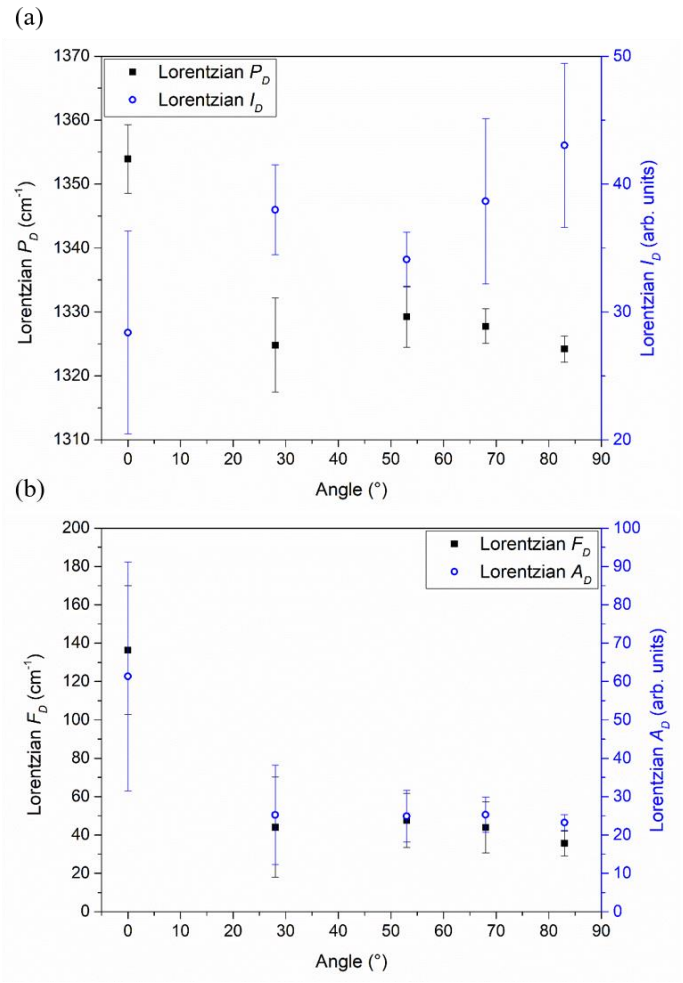

Figure 14: The evolution of the Lorentzian D peak against incident angle.

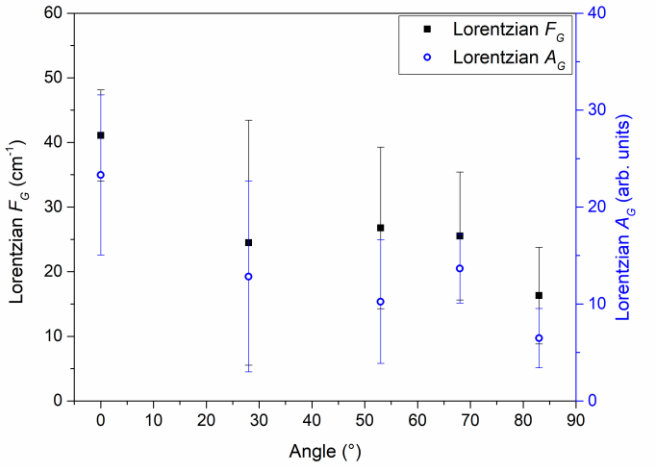

Figure 15: The evolution of the FWHM and integrated area of the Lorentzian G peak against incident angle.

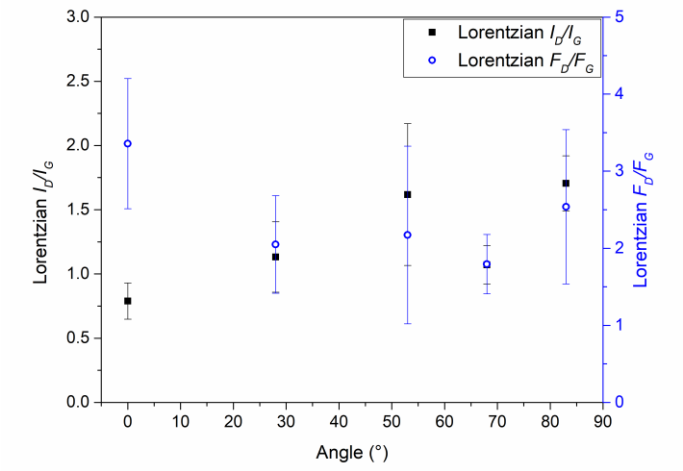

Figure 16: The evolution of the intensity ratio I_D/I_G and the FWHM ratio F_D/F_G against the incident angle.

4. Discussion

4.1 Treated Supported Graphene

SEM imaging of supported graphene samples shows that graphene has been completely sputtered off from the areas treated with 1×10^{-10} C/µm^2 (T100) and 5×10^{-11} C/µm^2 (T50) as evidenced by the lack of texture in these areas, i.e. no observable grain boundaries or patches of multilayer graphene. The characteristic D, G and 2D bands are also absent from the Raman spectra acquired from the mentioned areas.

Due to the relatively large size of the gallium ion, it is found that lower doses are required to sputter graphene then if helium ions were used [2, 10]. While helium ions pass right through the graphene with minimal damage and embed themselves in the SiO_2 substrate, gallium ions tend to transfer most of their kinetic energy to the surface of the sample and hence produce more damage in the top-most graphene layer [2]. Furthermore, molecular dynamics (MD) simulations [22] conclude that while heavier ions produce more damage, higher energies (on the order of 100 keV compared to 500 eV) induce less damage. Thus, heavier ions with lower energies are more efficient to mill uniformly shaped pores i.e. causing full sputtering in confined areas [22].

At treatment doses of 1×10^{-12} C/µm^2 (T1) and 5×10^{-13} C/µm^2 (T0.5), the 2D peak which is associated with the breathing mode of the graphene hexagonal ring is lost [18], implying that the graphene was transformed into amorphous carbon [5]. Raman spectra of carbon black

(amorphous carbon) consist of broad D and G peaks and a small broad bump at the 2D peak location [11], similar to what is observed in the above-mentioned treated supported graphene.

Various mechanisms can be attributed to the amorphization of the supported graphene sample. Firstly, the energetic ions hitting the graphene sample create defects, mostly point defects such as vacancies [5]. At low doses, these defects are sparse and only give rise to the activation of the disorder-induced D peak while the 2D peak is retained as the hexagonal crystal structure of the graphene is still mostly present, defined as Stage 1 [5]. At higher ion doses, the point defects start to coalesce to form more complex defects which will ultimately destroy the crystal structure of the graphene and hence the de-activation of the 2D peak, defined as Stage 2 [5]. In this case, the G and D peaks are still both present. The substrate supporting the graphene sheet can also be affected by the energetic ions [2, 23]. The size of the gallium ions precludes structural effects to the bulk of the substrate and thus causes a lot of disruption in the sample top-surface, even just below the graphene layer, forming serrations or very rough topographies of the underlying SiO_2 [24]. In turn, the disorder and roughness in the surface of the substrate supporting the graphene may increase the possibility of cracking and the formation of other associated defects which will de-crystallize and amorphize the graphene. This might be especially true for the areas treated with 1×10^{-12} C/μm^2 (T1) and 5×10^{-13} C/μm^2 (T0.5) as the topography and texture changed significantly. Finally, the atoms which have been sputtered from the graphene crystal structure to create vacancies can jump to another location to form adatoms and hence induce sp^3 hybridization. Similarly, the ion beam may be also depositing more carbonaceous material which may be present either in the chamber atmosphere or as contamination on the sample itself onto the graphene layer increasing the sp^3 hybridization [25]. In fact, Hong et al. [11] attribute the broad peaks induced by annealing to amorphous carbon deposited on graphene through carbonization of hydrocarbons during the applied thermal treatments in inert atmosphere [11]. In this work, the polymer transfer method used to transfer the CVD-grown graphene from the copper foil to the SiO_2 substrate is known to leave some polymer residue on the graphene sample – a precursor to carbonaceous material. Another contribution to the broad band at around 1300 cm^{-1} is the presence of organic contaminants which might be bound to the graphene causing chemical enhancement in the Raman spectrum [26, 27].

The ring of damaged graphene surrounding the 1×10^{-10} C/μm^2 (T100) area, also observed in [10], can be attributed to energetic ions from the ion beam which may have strayed from the focused beam and hit the graphene outside the target area. The presence of the D' peak at 1615 to 1623 cm^{-1} is in fact often attributed to the presence of point defects, for example created by argon ion beam sputtering [5, 28]. As the gallium ions impinge the sample, some ions might be backscattered and some atoms from both the graphene and the substrate might be sputtered inducing other defects, possibly away from the target area [7, 10, 23]. In fact, the majority of the total defects produced by an ion beam on supported graphene is attributed to indirect defect production [23]. Swelling of the substrate around the target area was also reported [2, 10].

The intensity ratio of $I_D/I_{D'}$ has been used to determine the defect type in graphene [6]. As shown in Figure 17, the $I_D/I_{D'}$ increases linearly from around 4.8 at a distance of around 20 μm when the peak can be first distinguished from the G peak, to around 8.6 at a distance of 60 um. We propose that closer to the treated area, the small $I_D/I_{D'}$ can be attributed more to boundary-like defects [6] brought about by extensive amorphization of the graphene and possible cracking due to the severe swelling of the substrate. As the distance away from the target area increases, these defects are replaced by vacancy-type defects caused by stray ions, and backscattering and sputtering actions resulting in a larger $I_D/I_{D'}$ [6]. The $I_D/I_{D'}$ is expected to vary gradually and the presence of the D′ peak at any point in the damaged zone can be attributed to a mixture of all the types of defects, from boundary defects to the presence of adatoms [10]. Song et al. [26] attribute peaks at relative shifts < 1550 cm^{-1} to materials bound to graphene which in our case could have originated from the polymer transfer process used or any other atmospheric contaminants. The $I_{D'}/I_G$ was also seen to increase closer to the target area until the D′ peak was no longer distinguishable from the G peak, as also reported in [6, 29].

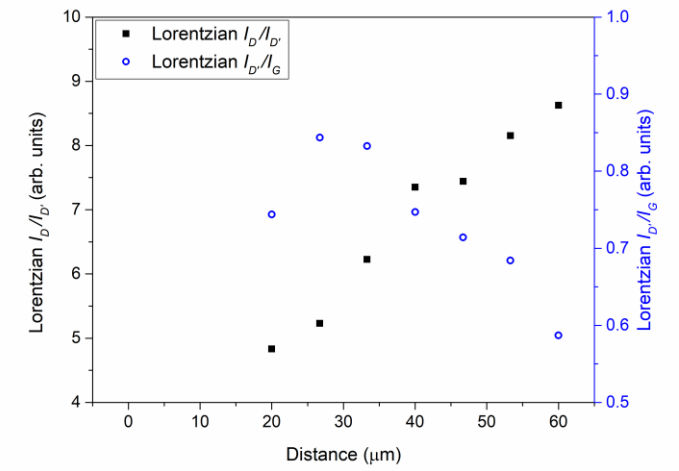

Figure 17: The evolution of the intensity ratio between the Lorentzian D and D' bands ($I_D/I_{D'}$) and the intensity ratio between the Lorentzian D' and G bands ($I_{D'}/I_G$).

One of the G peaks found at approximately 1530 cm^{-1}, previously attributed to the presence of amorphous carbon due to its Gaussian profile, evolves into a peak with a Lorentzian profile at lower defect concentrations. The G band is typically reported to split in two peaks with the presence of defects with the D' peak emerging at a higher frequency and often being attributed to the presence of point defects, for example created by ion beam sputtering [5]. The splitting of the G peak into two and the presence of multiple peaks in the wide region of 1150 to 1650 cm^{-1} was also related to strain in graphene, functionalization of graphene, and to the vibration of molecular oxygen [27, 30-33].

4.2 Treated Graphene Membranes

Clear trends relating the treatment dose applied to monolayer graphene membranes suspended over Quantifoil TEM grids to the Raman spectra are evident. These include the increase in the intensity [5] yet narrowing of the Lorentzian D peak with an increase in dose, and a decrease in intensity and broadening of the 2D peak. Both the Gaussian D and G peaks, and the Lorentzian G peak show a slight decrease in intensity. The slight upshift of the Gaussian G peak can be attributed to an increase in the disorder [21]. Furthermore, the I_{GG}/I_{GL} ratio (Figure 18 (a)), which was previously used to determine the degree of amorphization, shows a non-monotonic trend with respect to the dose in the suspended graphene. On the other hand, contrary to what was observed for supported graphene, the I_{DG}/I_{DL} ratio (Figure 18 (a)) decreases with an increase in the treatment dose. This may be attributed to the increase in Lorentzian D peak intensity while

the intensities of the Gaussian peaks do not significantly change. The intensity of the D peak and the Lorenztian I_D/I_G ratio increases linearly with an increase in the treatment dose, showing that defects are still being created in the graphene. MD simulations of suspended graphene under ion irradiation report that at low ion energies, comparable to those used in this study, the types of defects produced are most prominently single vacancies [14].

The two stages of low and high disorder as a result of ion bombardment mentioned previously have stemmed from a reported non-monotonic trend for the I_D/I_G [5]. While in Stage 1, the I_D/I_G ratio increases with an increase in the ion beam dose due to the introduction of defects, at higher doses, the graphene enters Stage 2 during which the defects start to coalesce, cause partial amorphization and hence a decrease in the I_D/I_G ratio. While it is reported that Stage 2 is reached with ion fluences as low as 10^{15} $Ar^+/\mu m^2$ [5], the I_D/I_G ratio in our study is not observed to decrease even with a treatment fluence of at least 7.6×10^{16} $Ga^+/\mu m^2$, indicating that the suspended graphene is still at Stage 1 disorder. As will be further discussed hereunder, we mainly attribute this discrepancy to the fact that the graphene in our work is suspended and not supported by a substrate. Another contributing factor to the absence of the non-monotonic trend in our I_D/I_G is the presence of both the Gaussian and Lorentzian D and G peaks. In fact, on examination of the total integrated area under the D and G peaks by adding both the Gaussian and Lorentzian components of each peak, A_D and A_G respectively in Figure 18 (b), we notice that both areas seem to peak at a fluence of 3×10^{15} $Ga^+/\mu m^2$ before they start to decay, in agreement with [5]. The laser used for the Raman measurements (1.96 eV) may also be a contributing factor to why this non-monotonic trend is not evidently observed as it has been reported that the non-monotonic trend of the I_D/I_G is less pronounced when using lower energy lasers [8].

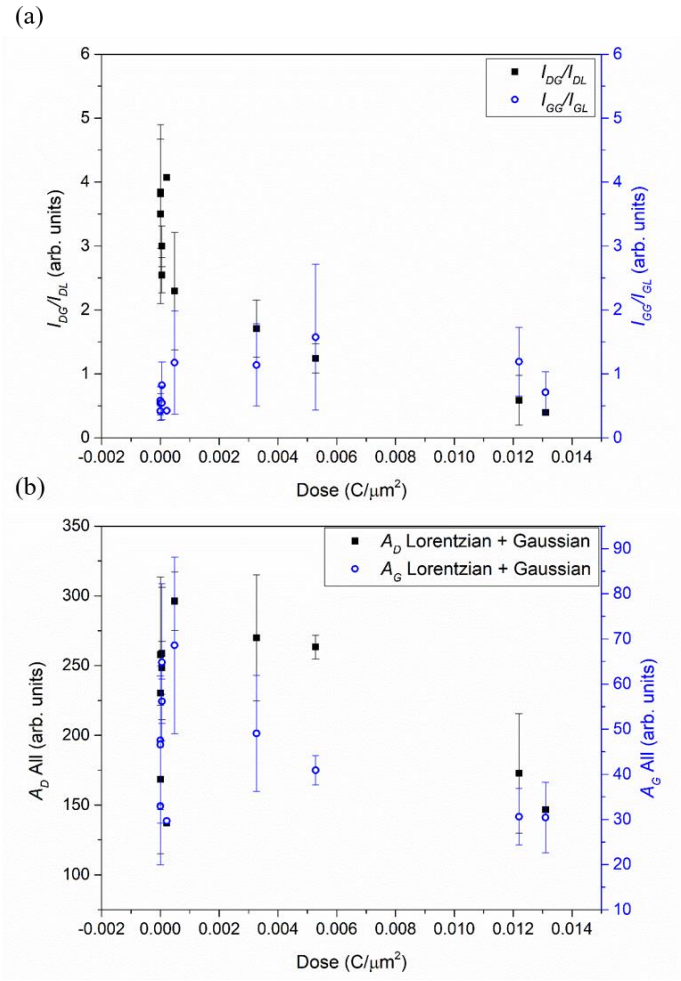

Figure 18: The evolution of (a) the intensity ratios I_{DG}/I_{DL} and I_{GG}/I_{GL}, and (b) the total integrated area A_D and A_G in suspended graphene.

As it stands, while lower treatment fluences from 1.12×10^{6} ions/μm^2 up to 6.24×10^{8} ions/μm^2 applied to supported graphene lead to partial amorphization or complete sputtering of graphene, higher fluences from 2.041×10^{12} ions/μm^2 up to 8.177×10^{16} ions/μm^2 applied to suspended graphene do not induce extensive amorphization. This is in agreement with the work by Fox et al. [7] who observe that supported graphene has a greater defect density I_D/I_G ratio than freestanding graphene for the same helium ion fluence. To be able to fairly compare the two cases, the accelerating voltage used must also be taken into consideration. In the suspended graphene, the same range of treatment dose was applied using both 5 kV and 30 kV (constant ion beam current of 1.5 pA), however, no discernible changes where seen in the Raman spectra.

Therefore, it is determined that this difference in accelerating voltage is insufficient to affect the extent of damage done by the ion beam on the supported graphene for the same dose [23].

This discrepancy in the effect of the same dose on different graphene samples is being attributed to the manner in which the graphene exists. The energetic ions impinging the supported graphene sample are able to pass through the graphene but are often trapped into the substrate causing swelling and roughening of the substrate. Some of the ions may also hit the substrate atoms and backscatter to the graphene from underneath causing double the damage [7, 10, 23]. On the other hand, the energetic ions impinging suspended graphene will only pass once through the graphene and then proceed to disperse in the atmosphere (or in the sample stage) with no backscatter. This means that the ions will only cause minimal damage mostly consisting of small vacancies. Furthermore, any carbon atoms from the graphene crystal structure which may have been knocked off the lattice will most likely be sputtered away into the atmosphere rather than implanted in the substrate or relocated as adatoms in the nearby graphene as expected in the supported graphene.

Similar results have been reported following MD simulations of argon and silicon ions hitting suspended and supported graphene [23, 34]. For a given dose at accelerating voltages lower than 5 keV, the energetic ions tend to produce more defects in suspended graphene rather than supported graphene since in the latter, the carbon atoms are supported by the substrate and more energy would be needed to sputter them. However, ions at higher accelerating voltages produce more defects in supported graphene [23].

The effect of the incidence angle on the damage imparted to the suspended graphene is also investigated. A treatment dose of 3.27×10^{-3} C/μm^2 was used and the incidence angle was changed from 28° to 83° to the sample surface. The Gaussian D and G peaks do not significantly change with the incidence angle. On the other hand, the intensity of the Lorenztian D peak and the Lorenztian I_D/I_G increase with an increase in the incidence angle. This indicates that as the incidence angle of the ion beam approaches 90° to the surface, more defects are being imparted in the graphene membrane, in agreement with simulation work [14]. This is attributed to the fact that at lower incidence angles the energetic ions graze the sample meaning that they split their transferred energy between the in-plane and out-of-plane directions. Therefore, less energy is available to knock off the carbon atoms in the out-of-plane direction hence creating less

vacancies. The grazing ions and any sputtered atoms might then bounce off the sample rather than get embedded into the substrate and so less indirect damage is produced. Grazing ions may create more Stone-Wales type defects since the carbon atoms would only be relocated or their bonds twisted.

5. Conclusion

In this work, the effect of ion irradiation on the Raman spectrum of graphene was investigated. A significant distinction between the response of the supported graphene and suspended graphene membranes to ion beam irradiation is reported, with the former experiencing more induced damage in response to lower beam doses. This is being attributed to indirect damage which is caused in the supported graphene due to backscattering and sputtering incidents, as well as substrate swelling. Full and partial amorphization of the supported graphene was also observed in the areas surrounding the directly irradiated areas. The ratio between the Gaussian D and Lorentzian D peaks (I_{DG}/I_{DL}) and the Gaussian G and Lorentzian G peaks (I_{GG}/I_{GL}) are being suggested to be used to quantify the degree of amorphization. A higher incidence angle of the ion beam to the suspended graphene surface increases the damage imparted in the graphene.

These results are relevant in the development of nanostructured membranes and nanoelectronics, for which ion beam irradiation may be used to impart controlled defects or precise sputtering of the graphene. The knowledge of the effect of the substrate on the final crystalline quality of the disordered graphene will determine the process adopted in the fabrication of graphene-based technologies. For instance, should nanopores be introduced in suspended graphene membranes via energetic particle beam irradiation with the scope of developing filtration or desalination membranes, whether the bombardment is to be applied before or after transferring the graphene membrane on the porous support membrane, needs to be considered.

6. References

[1] M. Wall, "The Raman spectroscopy of graphene and the determination of layer thickness," *Madison, WI Thermo Fisher Scientific* 2011.

[2] D. C. Bell, M. C. Lemme, L. A. Stern, J. R. Williams, and C. M. Marcus, "Precision cutting and patterning of graphene with helium ions," *Nanotechnology,* vol. 20, p. 455301, 2009.

[3] A. C. Ferrari, J. C. Meyer, V. Scardaci, C. Casiraghi, M. Lazzeri, F. Mauri, S. Piscanec, D. Jiang, K. S. Novoselov, S. Roth, and A. K. Geim, "Raman Spectrum of Graphene and Graphene Layers," *Physical Review Letters,* vol. 97, p. 187401, 2006.
[4] A. Reina, X. Jia, J. Ho, D. Nezich, H. Son, V. Bulovic, M. S. Dresselhaus, and J. Kong, "Large Area, Few-Layer Graphene Films on Arbitrary Substrates by Chemical Vapor Deposition," *Nano Letters,* vol. 9, pp. 30-35, 2009.
[5] M. M. Lucchese, F. Stavale, E. H. M. Ferreira, C. Vilani, M. V. O. Moutinho, R. B. Capaz, C. A. Achete, and A. Jorio, "Quantifying ion-induced defects and Raman relaxation length in graphene," *Carbon,* vol. 48, pp. 1592-1597, 2010.
[6] A. Eckmann, A. Felten, A. Mishchenko, L. Britnell, R. Krupke, K. S. Novoselov, and C. Casiraghi, "Probing the nature of defects in graphene by Raman spectroscopy," *Nano letters,* vol. 12, pp. 3925-3930, 2012.
[7] D. Fox, Y. B. Zhou, A. O'Neill, S. Kumar, J. J. Wang, J. N. Coleman, G. S. Duesberg, J. F. Donegan, and H. Z. Zhang, "Helium ion microscopy of graphene: beam damage, image quality and edge contrast," *Nanotechnology,* vol. 24, p. 335702, 2013.
[8] L. G. Cançado, A. Jorio, E. H. M. Ferreira, F. Stavale, C. A. Achete, R. B. Capaz, M. V. O. Moutinho, A. Lombardo, T. S. Kulmala, and A. C. Ferrari, "Quantifying Defects in Graphene via Raman Spectroscopy at Different Excitation Energies," *Nano Letters,* vol. 11, pp. 3190-3196, 2011.
[9] G. Compagnini, F. Giannazzo, S. Sonde, V. Raineri, and E. Rimini, "Ion irradiation and defect formation in single layer graphene," *Carbon,* vol. 47, pp. 3201-3207, 2009.
[10] S. Hang, Z. Moktadir, and H. Mizuta, "Raman study of damage extent in graphene nanostructures carved by high energy helium ion beam," *Carbon,* vol. 72, pp. 233-241, 2014.
[11] J. Hong, M. K. Park, E. J. Lee, D. Lee, D. S. Hwang, and S. Ryu, "Origin of New Broad Raman D and G Peaks in Annealed Graphene," *Scientific Reports,* vol. 3, p. 2700, 2013.
[12] A. Eckmann, A. Felten, I. Verzhbitskiy, R. Davey, and C. Casiraghi, "Raman study on defective graphene: Effect of the excitation energy, type, and amount of defects," *Physical Review B,* vol. 88, p. 035426, 2013.
[13] S. P. Surwade, S. N. Smirnov, I. V. Vlassiouk, R. R. Unocic, G. M. Veith, S. Dai, and S. M. Mahurin, "Water desalination using nanoporous single-layer graphene," *Nature nanotechnology,* 2015.
[14] O. Lehtinen, J. Kotakoski, A. V. Krasheninnikov, and J. Keinonen, "Cutting and controlled modification of graphene with ion beams," *Nanotechnology,* vol. 22, p. 175306, 2011.
[15] Nano Carbon Sp. z o.o. (2016, 26/07/2018). *Graphene on conductive SiO_2 / Si*. Available: https://www.grapheneshop.pl/product/graphene-conductive-sio2-si/?wcmlc=EUR
[16] Agar Scientific Ltd. (2018, 26/07/2018). *Suspended Monolayer Graphene on TEM Grids - Quantifoil*. Available: http://www.agarscientific.com/tem/support-films-graphene/suspended-monolayer-graphene-on-tem-grids-quantifoil.html
[17] C. A. Lieber and A. Mahadevan-Jansen, "Automated Method for Subtraction of Fluorescence from Biological Raman Spectra," *Applied Spectroscopy,* vol. 57, pp. 1363-1367, 2003.
[18] A. C. Ferrari and D. M. Basko, "Raman spectroscopy as a versatile tool for studying the properties of graphene," *Nature Nanotechnology,* vol. 8, p. 235, 2013.

[19] M. Pimenta, G. Dresselhaus, M. S. Dresselhaus, L. Cancado, A. Jorio, and R. Saito, "Studying disorder in graphite-based systems by Raman spectroscopy," *Physical chemistry chemical physics,* vol. 9, pp. 1276-1290, 2007.
[20] A. C. Ferrari and J. Robertson, "Interpretation of Raman spectra of disordered and amorphous carbon," *Physical review B,* vol. 61, p. 14095, 2000.
[21] A. Ferrari and J. Robertson, "Resonant Raman spectroscopy of disordered, amorphous, and diamondlike carbon," *Physical Review B,* vol. 64, p. 075414, 2001.
[22] W. Li, L. Liang, S. Zhao, S. Zhang, and J. Xue, "Fabrication of nanopores in a graphene sheet with heavy ions: A molecular dynamics study," *Journal of Applied Physics,* vol. 114, p. 234304, 2013.
[23] Z. Shijun, X. Jianming, W. Yugang, and Y. Sha, "Effect of SiO 2 substrate on the irradiation-assisted manipulation of supported graphene: a molecular dynamics study," *Nanotechnology,* vol. 23, p. 285703, 2012.
[24] R. Gago, L. Vázquez, R. Cuerno, M. Varela, C. Ballesteros, and J. M. Albella, "Nanopatterning of silicon surfaces by low-energy ion-beam sputtering: dependence on the angle of ion incidence," *Nanotechnology,* vol. 13, p. 304, 2002.
[25] K. N. Kudin, B. Ozbas, H. C. Schniepp, R. K. Prud'homme, I. A. Aksay, and R. Car, "Raman Spectra of Graphite Oxide and Functionalized Graphene Sheets," *Nano Letters,* vol. 8, pp. 36-41, 2008.
[26] J. Song, T. Y. Ko, and S. Ryu, "Raman spectroscopy study of annealing-induced effects on graphene prepared by micromechanical exfoliation," *Bulletin of the Korean Chemical Society,* vol. 31, pp. 2679-2682, 2010 2010.
[27] V. B. Mohan, M. Nieuwoudt, K. Jayaraman, and D. Bhattacharyya, "Quantification and analysis of Raman spectra of graphene materials," *Graphene Technology,* vol. 2, pp. 47-62, 2017.
[28] P. Ahlberg, F. Johansson, Z.-B. Zhang, U. Jansson, S.-L. Zhang, A. Lindblad, and T. Nyberg, "Defect formation in graphene during low-energy ion bombardment," *APL Materials,* vol. 4, p. 046104, 2016.
[29] Y.-B. Zhou, Z.-M. Liao, Y.-F. Wang, G. S. Duesberg, J. Xu, Q. Fu, X.-S. Wu, and D.-P. Yu, "Ion irradiation induced structural and electrical transition in graphene," *The Journal of Chemical Physics,* vol. 133, p. 234703, 2010.
[30] T. M. G. Mohiuddin, A. Lombardo, R. R. Nair, A. Bonetti, G. Savini, R. Jalil, N. Bonini, D. M. Basko, C. Galiotis, N. Marzari, K. S. Novoselov, A. K. Geim, and A. C. Ferrari, "Uniaxial strain in graphene by Raman spectroscopy: G peak splitting, Gruneisen parameters, and sample orientation," *Physical Review B,* vol. 79, p. 205433, 2009.
[31] M. Huang, H. Yan, C. Chen, D. Song, T. F. Heinz, and J. Hone, "Phonon softening and crystallographic orientation of strained graphene studied by Raman spectroscopy," *Proceedings of the National Academy of Sciences,* vol. 106, pp. 7304-7308, 2009.
[32] O. Frank, J. Vejpravova, V. Holy, L. Kavan, and M. Kalbac, "Interaction between graphene and copper substrate: The role of lattice orientation," *Carbon,* vol. 68, pp. 440-451, 2014.
[33] A. Sadezky, H. Muckenhuber, H. Grothe, R. Niessner, and U. Pöschl, "Raman microspectroscopy of soot and related carbonaceous materials: spectral analysis and structural information," *Carbon,* vol. 43, pp. 1731-1742, 2005.
[34] X. Wu, H. Zhao, and J. Pei, "Fabrication of nanopore in graphene by electron and ion beam irradiation: Influence of graphene thickness and substrate," *Computational Materials Science,* vol. 102, pp. 258-266, 2015.

7. Acknowledgments

This research was partially funded by the Endeavour Scholarship Scheme (Malta). This scholarship is part financed by the European Union European Social Fund (ESF) under Operational Programme II – Cohesion Policy 2014-2020, “Investing in human capital to create more opportunities and promote the well-being of society”. This research was part financed through the project “Collaborative Research on Nanomaterials” in the Internationalisation Partnership Award Scheme 2016, Malta Council for Science and Technology (MCST). The authors would like to acknowledge the technical support offered by the Nanobiotechnology Laboratories at the Consumer Products Safety, Directorate F – Health, Consumers and Reference Materials, Directorate General Joint Research Centre, European Commission, Italy.